# The early evolution of cranial appendages in Bovoidea revealed by new species of *Amphimoschus* (Mammalia: Ruminantia) from China

YI-KUN LI[1,2], BASTIEN MENNECART[3,4], MANUELA AIGLSTORFER[5], XI-JUN NI[6,7], QIANG LI[6,7,*] and TAO DENG[1,6,7,8,*]

[1]*Center for Research and Education on Biological Evolution and Environment, Nanjing University, Nanjing 210023, China*
[2]*State Key Laboratory of Palaeobiology and Stratigraphy, Nanjing Institute of Geology and Palaeontology, Chinese Academy of Sciences, Nanjing 210008, China*
[3]*Naturhistorisches Museum Basel, Basel 4001, Switzerland*
[4]*Naturhistorishes Museum Wien, Vienna 1010, Austria*
[5]*Naturhistorisches Museum Mainz / Landessammlung für Naturkunde Rheinland-Pfalz, Mainz 55116, Germany*
[6]*Key Laboratory of Vertebrate Evolution and Human Origins, Institute of Vertebrate Paleontology and Paleoanthropology, Chinese Academy of Sciences, Beijing 100044, China*
[7]*CAS Center for Excellence in Life and Paleoenvironment, Beijing 100044, China*
[8]*Department of Earth Sciences, University of Chinese Academy of Sciences, Beijing 100049, China*

The cranial appendage (headgear) is an iconic structure of modern ruminants, and four of the five extant pecoran families display morphological and physiological specialties. They probably share one origin from the same genetic basis, whereas the evolution of the cranial appendages is still debatable, especially in consideration of fossil taxa lacking headgear. *Amphimoschus* is an enigmatic pecoran that comprises no more than two species, mainly known from the late early/early middle Miocene of Western and Central Europe and considered not to possess any cranial appendages. Here, we present ***Amphimoschus xishuiensis* sp. nov.**, discovered in the Tabenbuluk area, Gansu Province, China. The new species reveals the first evidence of cranial ornamentations in the genus, including a supraorbital bump, an antorbital protuberance and frontal thickening. In our phylogenetic analysis the genus was inferred as a basal member of the Bovoidea, and thus the cranial ornamentations of *A. xishuiensis* might provide insight into the early evolution of cranial appendages in Bovoidea. They could be interpreted as weapons to defend territories in intense intraspecific or interspecific competition during the late early Miocene.

ADDITIONAL KEYWORDS:  cranium – Miocene – phylogeny – taxonomy – teeth.

## INTRODUCTION

Pecora constitutes most of the suborder Ruminantia and displays a great diversity of impressive cranial appendages (headgear). The cranial appendage on extant ruminants was recently resolved to have a single origin based on the common genetic and cellular basis and convergent but independent pseudogenization in Moschidae and Hydropotinae (Chen *et al.*, 2019; Wang *et al.*, 2019a). The striking morphological differences among extant ruminant families were interpreted as being attributable to minor evolutionary changes rather than non-homologous origins (Wang *et al.*, 2019a). However, a further correlation among those family-specific appendages remains unclear, particularly associated with fossil taxa (DeMiguel *et al.*, 2014). The diversification of modern families that mostly possess cranial appendages today has occurred during

*Corresponding authors. E-mail: dengtao@ivpp.ac.cn; liqiang@ivpp.ac.cn

the early and early middle Miocene (Gentry, 1994; Gentry *et al.*, 1999; Bibi, 2013; Mennecart *et al.*, 2017). A better knowledge of early pecorans will help to resolve their phylogenetic relationships and track the evolutionary development of this infraorder, which comprises one of the most successful groups of large mammals in ecosystem management (Bibi, 2014). Many early pecorans are little understood, and their phylogenetic positions are still under debate, such as *Dremotherium* Geoffroy, 1833 in the Cervoidea (Sánchez *et al.*, 2015) and *Bedenomeryx* Ginsburg, Morales & Soria, 1994 in the Giraffomorpha (Mennecart *et al.*, 2019). Pecoran radiation and early evolution were supposed to lie within Central Asia (Vislobokova, 1997; Gentry *et al.*, 1999), whereas ruminants from the early Miocene to early middle Miocene of China are relatively scattered, with eight genera currently reported (Chen & Wu, 1976; Li & Qiu, 1980; Li *et al.*, 1983; Qiu *et al.*, 1985, 2013; Wang *et al.*, 2003, 2009; Qiu & Qiu, 2013).

*Amphimoschus* Bourgeois, 1873 is an extinct ruminant commonly found in the late early/early middle Miocene [from Mammal Neogene zone (MN) 3 to MN 6] of Western and Central Europe (Mayet, 1908; Heizmann *et al.*, 1980; Gentry, 1994; Ginsburg & Bonneau, 1995; Gentry *et al.*, 1999; Mörs *et al.*, 2000; Ginsburg, 2001; Sach & Heizmann, 2001; Scherler *et al.*, 2013; Gagnaison, 2017; Mennecart *et al.*, 2021). Two species are generally recognized under the genus *Amphimoschus*: *Amphimoschus artenensis* Mayet, 1908 seems to be slightly smaller and older than the type species, *Amphimoschus ponteleviensis* Bourgeois, 1873 (Roman & Viret, 1934; Gentry, 1994; Gentry & Heizmann, 1996). However, after a broad and comprehensive re-examination, Mennecart *et al.* (2021) have shown that both fall in the intraspecific variability of *A. ponteleviensis*. Besides its provenance in Europe, the genus *Amphimoschus* is also mentioned in China as *Amphimoschus* sp. from Xiacaowan of Jiangsu Province (Li *et al.*, 1983) and as *Amphimoschus* cf. *A. artenensis* from Xishuigou of Gansu Province (Wang *et al.*, 2003, 2008). Unfortunately, there is no comprehensive description so far, and the former is unavailable. Here, we provide the first comprehensive description of *Amphimoschus* material from China based on historical and new collections, including a hemimandible with a complete postcanine tooth row, two maxillae and one partial skull. The unique combination of dental characters shows a close affinity with the European *Amphimoschus*, and the partial skull shows the first indication of cranial ornamentations in the genus.

## MATERIAL AND METHODS

The material described in this paper was excavated during field expeditions in the Tabenbuluk area in years 1999, 2014 and 2015 (Fig. 1). The material is now deposited in the collection of the Institute of Vertebrate Paleontology and Paleoanthropology, Chinese Academy of Sciences (Beijing, China).

The right hemimandible and partial skull were scanned using 225 kV micro-computerized tomography at the Key Laboratory of Vertebrate Evolution and Human Origins, Chinese Academy of Sciences. The hemimandible was scanned with a beam energy of 140 kV and a flux of 120 µA at a resolution of 63 µm per pixel, using a 360° rotation with a step size of 0.5°, and the partial skull was scanned with 160 kV energy and 120 µA flux at 59.6 µm per pixel resolution. A total of 720 projections were reconstructed in a 2048 × 2048 matrix of 1536 slices using the two-dimensional reconstruction software (Wang *et al.*, 2019b). Segmentation and digital reconstruction were carried out with the software MIMICS RESEARCH (v.20.0), and the reconstruction is on open access on the MorphoMuseuM website (https://doi.org/10.18563/journal.m3.151, Li *et al.*, 2021b).

The phylogenetic analysis was based on the data matrix of Mennecart *et al.* (2021), and the character type, character state optimization and outgroups followed their proposed settings. Three characters were added to that data matrix and consisted of the presence or absence of p1, presence or absence of labial sulcus on p4, and alignment of lingual cuspids of lower molars. Those three characters correspond to characters 30, 34 and 38, respectively, of Sánchez *et al.* (2015). The genus *Amphimoschus* replaced the taxon *A. ponteleviensis* here, because the new species, *Amphimoschus xishuiensis*, was integrated into the character coding. Thus, character 43 changed to state 1 and 2, and character 51 changed to state 0 and 1 in *Amphimoschus*. Besides that genus, the other 18 species and 68 characters formed the data matrix (Supporting Information, File S1). The new topological constraints were modified from the genomic backbone of nine extant species of Chen *et al.* (2019) combined with the extinct species *Procervulus dichotomus* (Gervais, 1849). The analysis was carried out with the software PAUP v.4.0a (Swofford, 2002), using a heuristic search with the random addition sequence of 1000 replicates and 100 trees saved per replication. The bootstrap value was calculated by 1000 replicates with the random addition sequence of 100 replicates, and Bremer support was calculated by searching trees longer than the most parsimony until all branches collapsed.

The ancestral reconstruction was based on the bovid and moschid typology proposed by Chen *et al.* (2019), consisting of 39 extant species. Male territories were modified from Bärmann (2014) and contained three states defined as the following: living in permanent territories (state 0); establishing temporary territories during the rut or showing territories on some
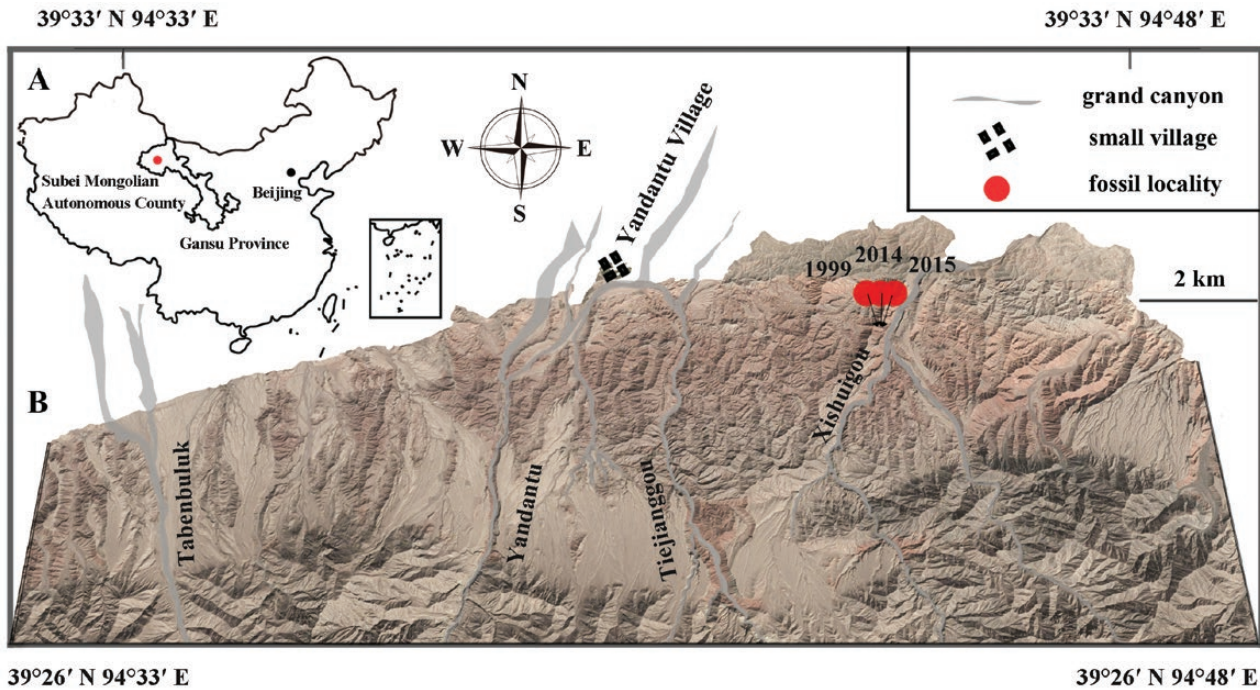
**Figure 1.** Location where *Amphimoschus xishuiensis* was found in the Xishuigou, Tabenbuluk area, Gansu Province, China. A, administrative map of China, with the outline of Gansu Province (China basemap after China National Bureau of Surveying and Mapping Geological Information). B, simplified topographical map (modified from screen shot at Tabenbuluk area in Google Earth, December 2012, eye altitude = 28 km).

occasions or proportions (state 1); and not establishing territories (state 2). The behavioural data of extant species were based mainly on the studies by Jarman (1974) and Castelló (2016) (Supporting Information, File S2, Table S1). The ancestral reconstruction was analysed by using maximum likelihood in the software MESQUITE (v.3.40), with the default probability method (Maddison & Maddison, 2018).

Terminology and nomenclature for teeth follow Bärmann & Rössner (2011) and those for the skull follow Barone (1999). Measurements were taken using digital callipers with accuracies of 0.1 mm on the teeth and 0.5 mm on the skull owing to taphonomic processes.

ABBREVIATIONS

Abbreviations are as follows: DH, suffix of IVPP Danghe locality numbers; IVPP V or V, suffix of specimen from Institute of Vertebrate Paleontology and Paleoanthropology; M/m and P/p, upper/lower molar and premolar, respectively; PIMUZ, suffix of specimen from Paläontologische Museum der Universität Zürich, Switzerland; T. b., suffix of Tabenbuluk specimen in Birger Bohlin Collection. Conventional abbreviations used in front of the year in the synonymy list follow Matthews (1973): v, the authors have seen the original material of the reference.

SYSTEMATIC PALAEONTOLOGY

ORDER ARTIODACTYLA OWEN, 1848

SUBORDER RUMINANTIA SCOPOLI, 1777

INFRAORDER PECORA FLOWER, 1883

GENUS *AMPHIMOSCHUS* BOURGEOIS, 1873

*Type species: Amphimoschus ponteleviensis* Bourgeois, 1873.

*AMPHIMOSCHUS XISHUIENSIS* SP. NOV.

v 2003 *Amphimoschus* cf. *A. artenensis* Wang *et al.*: 262.

v 2008 *Amphimoschus* cf. *A. artenensis* Wang *et al.*: 3, fig. 8.

*Zoobank registration:* urn:lsid:zoobank. org:act:716C1F0F-1F6E-4112-8960-C0DB3AB67F9A

*Holotype: IVPP V 25521.1*, a right hemimandible with tooth row p2–m3, discovered from the site DH199911 (39°29′24.0″N, 94°43′52.8″E) in 1999, equivalent to the localities of T. b. 312–313 (Bohlin, 1946) and previously attributed to *Amphimoschus* cf. *A. artenensis* (Wang *et al.*, 2003, 2008).

*Referred material:* IVPP V 25521.2, anterior part of a skull with right P4–M3 and left P3–M2, from the site in 2015 (39°29′25.0″N, 94°43′52.6″E); V 25521.3, left maxilla with partial P3–M3, from the site in 2014 (39°29′24.7″N, 94°43′53.0″E); V 25521.4, right maxilla with M2 and M3 from the site DH199911, previously attributed to *Amphimoschus* cf. *A. artenensis* (Wang *et al.*, 2003, 2008).

*Type locality:* Xishuigou, East gully of the Tabenbuluk area, Subei Mongolian Autonomous County, Gansu Province, China.

*Associated fauna and age:* Xishuigou fauna, proposed by Wang *et al.* (2008) and comprising '*Kansupithecus*', *Platybelodon dangheensis* Wang & Qiu, 2002, *Turcocerus halamagaiensis* (Ye, 1989), *Kinometaxia guangpui* Wang, 2004 and *Heterosminthus intermedius* Wang, 2003 (Bohlin, 1946; Wang, 2002; Wang & Qiu, 2002; Wang *et al.*, 2004; Li *et al.*, 2021a); Tiejianggou Formation, ~17.0–19.7 Mya, late early Miocene (Wang *et al.*, 2013).

*Etymology:* Species name attributed to the fossil locality Xishuigou (Xishui gully).

*Differential diagnosis:* On average, larger in size than European *Amphimoschus* (*A. ponteleviensis*), *A. xishuiensis* possesses a smaller lower premolar/molar ratio than any known specimen of *A. ponteleviensis*. *Amphimoschus xishuiensis* differs from *A. ponteleviensis* in having a relatively compressed p4 with narrow anterior valley and broad transverse cristid, a well-developed metastylid on m1–m3, an additional stylid at the lingual base on m1–m2, an anterolingual cingulum on P4, and the presence of cranial ornamentations, including a supraorbital bump, an antorbital protuberance and frontal thickening.

## Description

*Cranium:* Only the right facial part is relatively well preserved in the skull V 25521.2 (Fig. 2), which suffers from post-mortem deformation and possesses posterior–lateral to anterior–medial and transversal cracks at the dorsal and anterior parts. The nasal bones could be separated easily and seem to form a semicircular pipe, and they share a U-shaped suture line with the frontal. The antorbital vacuity is present posteriorly to the nasal and situated in a relatively anterior position, whereas its shape is unclear to define. The frontal bones are distinctly thickened, starting from the suture between the nasal and the frontal and ending with a rounded protuberance.

The protuberance is located 10.9 mm anterior to the anterior orbital margin, and within this distance a ridge is present, connecting the protuberance to the orbit. The right orbit might not be circular in shape, given that its dorsal and posterior margins are less curved. The orbital length (32.3 mm) is slightly larger than its height (29.2 mm), but it is compressed dorsoventrally and lateromedially. A small supraorbital bump is situated centrally at the outer edge of the dorsal orbital margin, and it shows a bony fibrous internal structure consisting of thin, compact cortical and thick, spongy central regions, similar to the antorbital protuberance (Fig. 2B). Only the anterior part of the frontal midline is still in place, which is straight and simple. Its adjacent region is relatively flat and horizontal, whereas the posterior frontal is slightly elevated. A prominent ridge is present at the posterior part of the frontal, connecting the parietal to the orbit. The ventral orbital margin is robust, as is the preserved temporal process, indicating that the zygomatic is well developed. The facial region anterior to the orbit is long and flat; hence, the lacrimal fossa is absent. The bony surface of the maxilla is mostly exposed. The dorsal half of the maxilla, connected to the nasal, forms a smooth bulky relief, increasing the depression between the nasal and the maxilla.

*Upper teeth:* The enamel of the teeth is wrinkled. The M1 of IVPP V 25521.2 and 25521.3 is heavily worn, indicating that those specimens belong to adult individuals. V 25521.4 had a similar age at death, because it possesses a similar stage of wear to V 25521.3 (Fig. 3). The length of the upper molar row of V 25521.3 is estimated at 45 mm. The length of M1–M2 in V 25521.3 is 29.8 mm, and that of M2–M3 in V 25521.4 is 30.2 mm. The P3 is fragmentary in IVPP V 25521.2 and 25521.3. The lingual cone is located almost centrally, slightly shifted posteriorly, with a slightly convex posterolingual crista. The labial cone is broken, whereas it possesses a developed labial rib. The posterolabial crista is shorter than the posterolingual one. The labiolingually oriented central fold separates the fossa into anterior and posterior parts. The outline of the P4 is triangular, with a rounded lingual portion. The labial cone is large, and the anterolabial and posterolabial cristae are short and parallel to the anteroposterior direction. The labial cone rib is moderately developed and located centrally. The labial cone is more slender but higher than the lingual one. The lingual cone is located almost centrally and shifted only slightly to the posterior. The anterior and posterior styles are moderately developed. There is a central fold that forms an enamel bulge on the posterior part of the fossa. The anterolingual cingulum is present and constricted anterior to the lingual cone in V 25521.3, whereas in V 25521.2, the cingulum surrounds the lingual cone. The outline of the
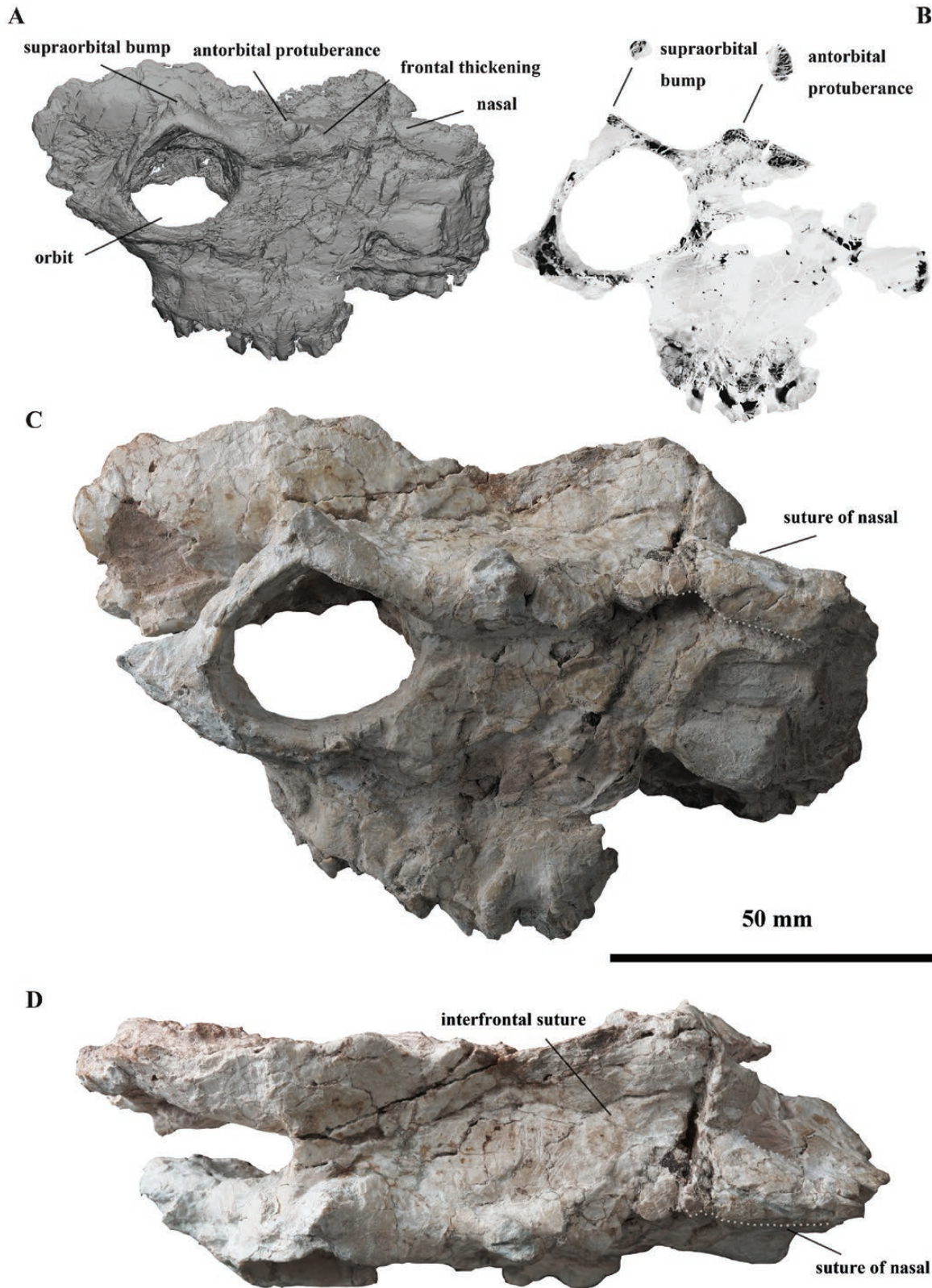
**Figure 2.** Skull of *Amphimoschus xishuiensis* from Tabenbuluk area, China. A, right lateral view of computed tomography (CT) reconstruction of IVPP V 25521.2 (3D models seen in Li *et al.*, 2021b). B, CT scanning screenshots of sagittal view at slice 1115.1, axial view at slice 8158.5, and axial view at slice 6961.5. C, right lateral view. D, dorsal view. Scale bar applies to C and D.
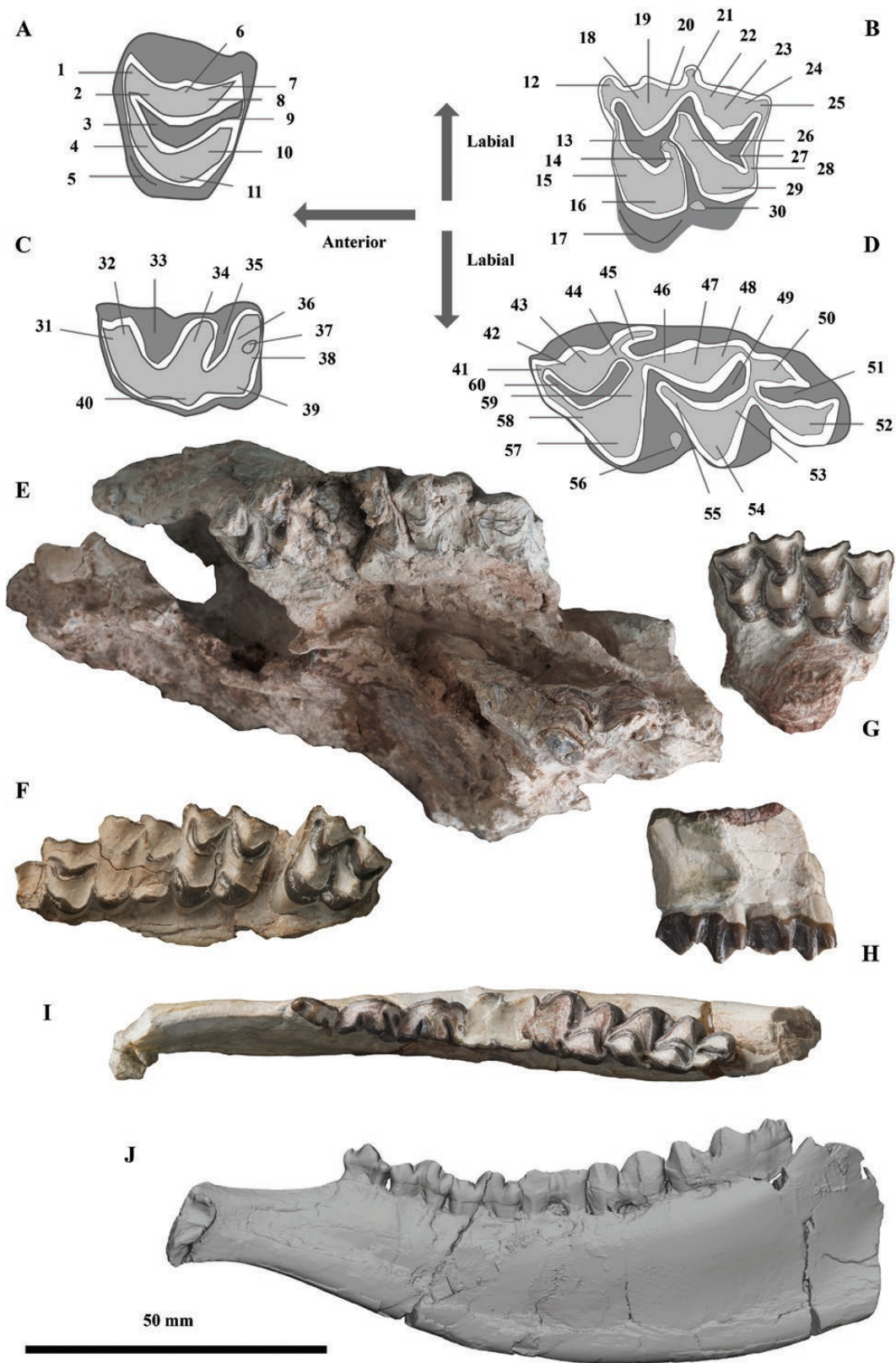
**Figure 3.** Dental nomenclature and cheek teeth of *Amphimoschus xishuiensis* from Tabenbuluk area, China. A, upper premolar: 1, anterior style; 2, anterolabial crista; 3, fossa; 4, anterolingual crista; 5, anterolingual cingulum; 6, labial cone; 7,

upper molars is relatively square. The M2 and M3 are of similar length. Owing to heavy wear, the main cusps of the M1 are flat. On M2 and M3 of IVPP V 25521.3 and 25521.4, the labial end of the straight postprotocrista is not bifurcated but instead turns anteriorly; however, it is bifurcated on M3 of V 25521.2. The labial end of the postprotocrista reaches the posterolingual base of the paracone that forms a small internal enamel fold into the anterior fossa. The metaconule is similar in size to the protocone on M1 and M2, whereas it is smaller than the protocone on M3. The preprotocrista, similar to the premetaconulecrista, is anterolabially oriented. The preprotocrista joins the parastyle on its lingual side, enclosing the anterior fossa, and the postmetaconulecrista joins the small metastyle, enclosing the posterior fossa posteriorly. The postmetaconulecrista bears a metaconule fold. The straight premetaconulecrista is not connected to any crista on its labial end, where a small bifurcation is present. On heavily worn teeth, the lingual branch of that bifurcation fuses with the postprotocrista, forming an enamel island at mid-length. The paracone rib is moderately developed and the metacone rib less developed. The metacone wall is inclined posteriorly relative to the paracone wall on M1 and M2 and slightly less inclined on M3. The labial cristae are short. On M1 and M2, the postparacrista reaches the labial end of the premetacrista, and there is no fusion on M2. The parastyle and metastyle are more developed from M1 to M3. The mesostyle is well developed and anteriorly directed on M1, anterolabially directed on M2, and slightly smaller and labially directed on M3. On M1 and M2, the mesostyle meets the premetacrista only, but it seems to combine the postparacrista and premetacrista on M3. The entostyle is large and trapezoidal on M1 and M2 but is smaller and ovoid on M3. The entostyle is fully isolated on M3, whereas its margin fuses with the premetaconulecrista entirely on M1 and slightly on M2. A faint and small posterior cingulum is present on M1 of V 25521.2. Anterior and lingual cingula are present on M2 and M3, separated by the protocone on M2 but connected and surrounding the protocone on M3.

*Hemimandible:* The hemimandible (*V 25521.1*) is relatively stocky, with a high corpus mandibulae (Fig. 3I, J). The height of the corpus mandibulae anterior to the m3 is 27.9 mm, and it gradually decreases in height to only 19.6 mm anterior to the p2. A small crest is present anterior to the p2. The distance between the symphysis and p2 is about as long as the premolar row.

*Lower teeth:* The complete cheek tooth row is preserved in *V 25521.1*, with 73.6 mm length (Fig. 3I, J). The ratio between lower premolar and molar rows is 0.65 (lower premolar row 29.5 mm; lower molar row 45.5 mm). The enamel is wrinkled on all teeth. The m1 is heavily worn, indicating that the specimen belongs to an adult individual. The lower premolars share the basic structure, with a more complex pattern from p2 to p4. The p3, the p4 and the posterior portion of p2 are strongly worn. The premolars become longer from p2 to p4. The p2 has an elongated triangular outline in the occlusal view, whereas the p3 and p4 are more enlarged in the anterior portion. The p4 is stocky. The anterior conid is small and anterolingually directed on p2 and is larger and more lingually directed on p3 and p4. It protrudes less lingually than the mesolingual conid on p2 and p3, but more-or-less at the same axis as the mesolingual conid on p4. The anterior valley forms a more acute angle from p2 to p4. Only the p3 and p4 possess an anterior stylid, which is small and directed lingually. The anterolabial cristid is short and anterolingually oriented. The mesolabial conid is positioned anteriorly on p2 to centrally on p4, and it is the highest cuspid of the lower premolars. On p2, the mesolabial conid is situated slightly more lingually than the posterolabial conid, and the groove anterior to the posterolabial conid is shallow. On p3 and p4, the mesolabial conid is situated more labially than the posterolabial conid, and that groove on p4 is more profound than on p3. There is no distinct mesolingual conid. The transverse cristid is more prolonged and broader from p2 to p4 and is of similar posterolingual orientation. The posterolingual conid on p2 seems short, ending in the middle part of the tooth, whereas it forms the posterolingual end on p3 and p4. The posterolingual conid protrudes more lingually than the transverse cristid on p3 and p4. The posterior stylid is long on p2 and reaches the lingualmost side

posterior style; 8, posterolabial crista; 9, central fold; 10, posterolingual crista; 11, lingual cone. B, upper molar: 12, parastyle; 13, anterior fossa; 14, postprotocrista; 15, preprotocrista; 16, protocone; 17, anterior and lingual cingula; 18, preparacrista; 19, paracone; 20, postparacrista; 21, mesostyle; 22, premetacrista; 23, metacone; 24, postmetacrista; 25, metastyle; 26, premetaconulecrista; 27, posterior fossa; 28, postmetaconulecrista; 29, metaconule; 30, entostyle. C, lower premolar: 31, anterior stylid; 32, anterior conid; 33, anterior valley; 34, transverse cristid; 35, posterior valley; 36, posterolingual conid; 37, back valley; 38, posterior stylid; 39, posterolabial conid; 40, mesolabial conid. D, lower molar: 41, mesostylid; 42, premetacristid; 43, metaconid; 44, postmetacristid; 45, metastylid; 46, pre-entocristid; 47, entoconid; 48, postentocristid; 49, posterior fossa; 50, entoconulid; 51, back fossa of m3; 52, hypoconulid; 53, posthypocristid; 54, hypoconid; 55, prehypocristid; 56, ectostylid; 57, protoconid; 58, preprotocristid; 59, postprotocristid; 60, anterior fossa. E, occlusal view of IVPP V 25521.2. F, occlusal view of V 25521.3. G, occlusal view of V 25521.4. H, labial view of V 25521.4. I, occlusal view of *V 25521.1*. J, lingual view of computed tomography reconstruction of *V 25521.1* (3D models seen in Li *et al.*, 2021b). Scale bar applies to E–J.

of the tooth. On p3 and p4, it is shorter and joins the posterolingual conid on its posterior half. There is no cingulid in any premolar. The molars are longer from m1 to m3. The lingual wall on m1 is relatively flat. The metaconid rib, stronger from m1 to m3, is more developed than the corresponding entoconid rib. In the occlusal view, the entoconid is lingually flattened, with straight and short cristids. The metastylid, starting from the middle of the postmetacristid, is well developed and more posteriorly elongated from m1 to m3. On m3, it even forms a fold covering the anterior portion of the pre-entocristid. The postmetacristid, pre-entocristid and internal postprotocristid are fused together on the lingual half of the teeth. There is no external postprotocristid in any molar. The preprotocristid is elongated, curved and fused with the premetacristid, which is short and straight. Owing to heavy wear, the prehypocristid fuses a little with the lingual part of the internal postprotocristid on m2, whereas on m3 it is lingually isolated. The posthypocristid is straighter from m1 to m3 because the posterior tooth is less protruding than the anterior one. The posthypocristid reaches the lingual side of m2 (not observed on m1 owing to wear), enclosing the posterior fossa; however, there is no direct fusion between the postentocristid and posthypocristid. The third basin of m3 is well structured. The entoconulid is well developed, elongated and globular and forms a bulgy lingual part of the back fossa. The entoconulid connects with the postentocristid on its anterolingual part and the posthypocristid on its anterolabial part. The short postentoconulidcristid does not join the posthypoconulidcristid, which leaves the posterior part of the back fossa open. The hypoconulid is large, and the prehypoconulidcristid fuses with the posthypocristid in the lingual mid-length. The back fossa of m3 is narrow, anteroposteriorly oriented and posteriorly open. An additional stylid occurs at the lingual base of the junction between the metaconid and entoconid, and that stylid is well developed on m1 and m2, forming a small column, and is smaller on m3. The ectostylid is well developed, high, elliptic and oblique in shape on m2, and smaller and rounded on m3 in the occlusal view. The posterior ectostylid is vestigial. The anterior cingulid is not observed on m1 owing to wear but is weakly present on m2 and m3.

## Comparison

Only one type of low-crowned ruminant dentition was discovered from Xishuigou, Tabenbuluk area, and the upper and lower cheek teeth were consistent in dimensions and morphology (Fig. 3; Table 1). The ruminant could be assigned to the genus *Amphimoschus* owing to the following character combination: (1) well-developed ectostylid on lower

**Table 1.** Measurements (in millimetres) of cheek teeth of *Amphimoschus xishuiensis*

| Specimen no. | Type | Length | Width at anterior lobe | Width at posterior lobe | Width at third lobe | Height 1 | Height 2 | Height 3 |
|---|---|---|---|---|---|---|---|---|
| V 25521.1 | Right p2 | 8.9 | 3.9 | 4.9 | – | 4.1 | 2.1 | – |
| | Right p3 | 10.5 | 5.8 | 5.9 | – | 4.5 | 4.0 | – |
| | Right p4 | 11.0 | 7.5 | 7.2 | – | 5.2 | 3.9 | – |
| | Right m1 | 11.3 | 10.4 | – | – | 4.3 | 3.1 | – |
| | Right m2 | 14.9 | 11.3 | 10.8 | – | 5.2 | 5.7 | – |
| | Right m3 | 21.8 | 10.6 | 10.1 | 7.7 | 6.7 | 7.5 | 5.7 |
| V 25521.2 | Right P4 | – | – | – | – | 8.2 | – | – |
| | Right M3 | 15.7 | | 14.0 | | 9.9 | 9.1 | – |
| V 25521.3 | Left P4 | 10.2 | 12.7 | – | – | 6.1 | – | – |
| | Left M1 | 13.8 | 15.0 | 13.6 | – | 4.6 | 4.9 | – |
| | Left M2 | 16.2 | 17.1 | 16.1 | – | 7.4 | 6.7 | – |
| | Left M3 | 16.1 | 16.3 | 14.0 | – | 8.2 | 7.1 | – |
| V 25521.4 | Right M2 | 15.5 | 17.1 | 15.8 | – | 7.5 | 6.9 | – |
| | Right M3 | 15.6 | 16.1 | 14.1 | – | 8.1 | 7.2 | – |

For lower teeth, Height 1 means the height at the metaconid (mesolingual conid), Height 2 means the height at the entoconid (posterolingual conid), and Height 3 means the height at the entoconulid; for upper teeth, Height 1 means the height at the paracone, and Height 2 means the height at the metacone.

molars/entostyle on upper molars; (2) lack of external postprotocristid (*Palaeomeryx* fold), (3) the third lobe of m3 double crescentic, with strongly developed entoconulid; (4) conspicuously wrinkled enamel; and (5) massive mandible and cranium (Bourgeois, 1873; Mayet, 1908; Mennecart *et al.*, 2021). The genus *Amphimoschus* was erected by Bourgeois in 1873 and recently amended by Mennecart *et al.* (2021). The material from Xishuigou can be distinguished from *A. ponteleviensis* by the presence of the supraorbital bump, antorbital protuberance and frontal thickening on the cranium, which provides the first evidence of the cranial ornamentation of the genus. Furthermore, the material from Xishuigou differs from *A. ponteleviensis* in the small lower premolar/molar ratio, the presence of a relatively compressed p4 with narrow anterior valley and broad transverse cristid, a well-developed metastylid on m1–m3, an additional lingual stylid on m1 and m2, and an anterolingual cingulum on P4. Based on the above differences, a new species, *A. xishuiensis*, is erected.

## RESULTS

### PHYLOGENETIC ANALYSIS

The phylogenetic analysis was principally based on the data matrix of Mennecart *et al.* (2021) and modified with three newly added characters and a new topological constraint (Supporting Information, File S1). Parsimony analysis returned nine most parsimonious trees. The most parsimonious tree equalled 232 steps when the gaps were treated as missing and the multiple states were interpreted as polymorphism, and it equalled 234 steps when those states were interpreted as uncertainty. The strict consensus tree retained the backbone constraints (Fig. 4), keeping the basic topology of ((Antilocapridae, Giraffidae), (Cervidae, (Bovidae, Moschidae))), as indicated by the genome phylogenetic analysis (Chen *et al.*, 2019). *Amphimoschus* was recovered as a sister group of the clade that encompassed the extant and extinct species of Bovidae and Moschidae. Seven synapomorphies supported this branch [characters 15 (0), 28 (0), 36 (0), 43 (2), 45 (1), 53 (1) and 68 (1); Supporting Information, File S2, Fig. S1]. Of these, the capitular facet in the radius being elongated and wide [character 53 (1)] is the strict synapomorphy of this branch, whereas it is unknown in *Amphimoschus*.

The systematic position of *Amphimoschus* was controversial, situated within the Hoplitomerycidae as a member of Cervoidea (Janis & Scott, 1987), close to the Antilocapridae (Mennecart *et al.*, 2021) or regarded as the sister group of Bovidae separately (Gentry, 1994) or together with *Moschus* Linnaeus, 1758 within the Moschidae (Rössner *et al.*, 2013).

The family Hoplitomerycidae was erected based on *Hoplitomeryx matthewi* Leinders, 1983 and comprised European genera *Hoplitomeryx* Leinders, 1983 and *Amphimoschus* (Janis & Scott, 1987). However, recent revision excluded its systematic attribution from the Cervoidea, and the proposed cervoid characters, including the double lacrimal orifice and closed metatarsal gully, were not exclusive in the family Cervidae (Mazza, 2013). Gentry (1994) first proposed that *Amphimoschus* might be a sister group of Bovidae rather than of Cervidae because the protoconal fold was not a consistent character present in the upper molar. Besides the protoconal fold, *Amphimoschus* differs from Cervidae in the absence of the lacrimal fossa (Janis & Scott, 1987). It differs from Antilocapridae in the presence of upper canines and well- or weakly developed metastylids on lower molars (Janis & Manning, 1998) and further differs from Moschidae in the simple p4, without antero- and posterolingual cristids, and a weakly developed postentoconulidcristid at the third lobe of m3 (Sánchez *et al.*, 2010). Sánchez *et al.* (2010) amended the diagnosis of the Bovoidea, and *Amphimoschus* shares with these the developed postentocristid that fuses with the posthypocristid, an expanded postprotocristid, the absence of a lacrimal fossa, and aligned cuspids on lower molars. Thus, *Amphimoschus* might be a basal member of the Bovoidea.

## DISCUSSION

### EARLY EVOLUTION OF CRANIAL APPENDAGES IN BOVOIDEA

Neglecting headgearless fossil taxa when studying the evolution of cranial appendages in ruminants might lead to misinterpretations and is predestined to miss out on the real origin of these appendages (Davis *et al.*, 2011; DeMiguel *et al.*, 2014). *Amphimoschus* was previously treated as a headgearless ruminant (Janis & Scott, 1987) and recently doubted by Mennecart *et al.* (2021) based on the presence of strong supraorbital ridges on specimen PIMUZ A/V4656. The presence of the supraorbital bump on specimen V 25521.2 of *A. xishuiensis* confirms the first evidence of headgear in this genus. The supraorbital bump is broken at its tip, and the preserved morphology does not allow assignation to any of the specific pecoran structures. The phylogenetic analysis proposes that *Amphimoschus* is a basal member of the Bovoidea; hence, the supraorbital bump could be viewed as the initial development of a horn-like appendage, being positioned between developmental stage C2 and C3 of Bubenik (1990). Besides the supraorbital bump, *A. xishuiensis* possesses an antorbital protuberance
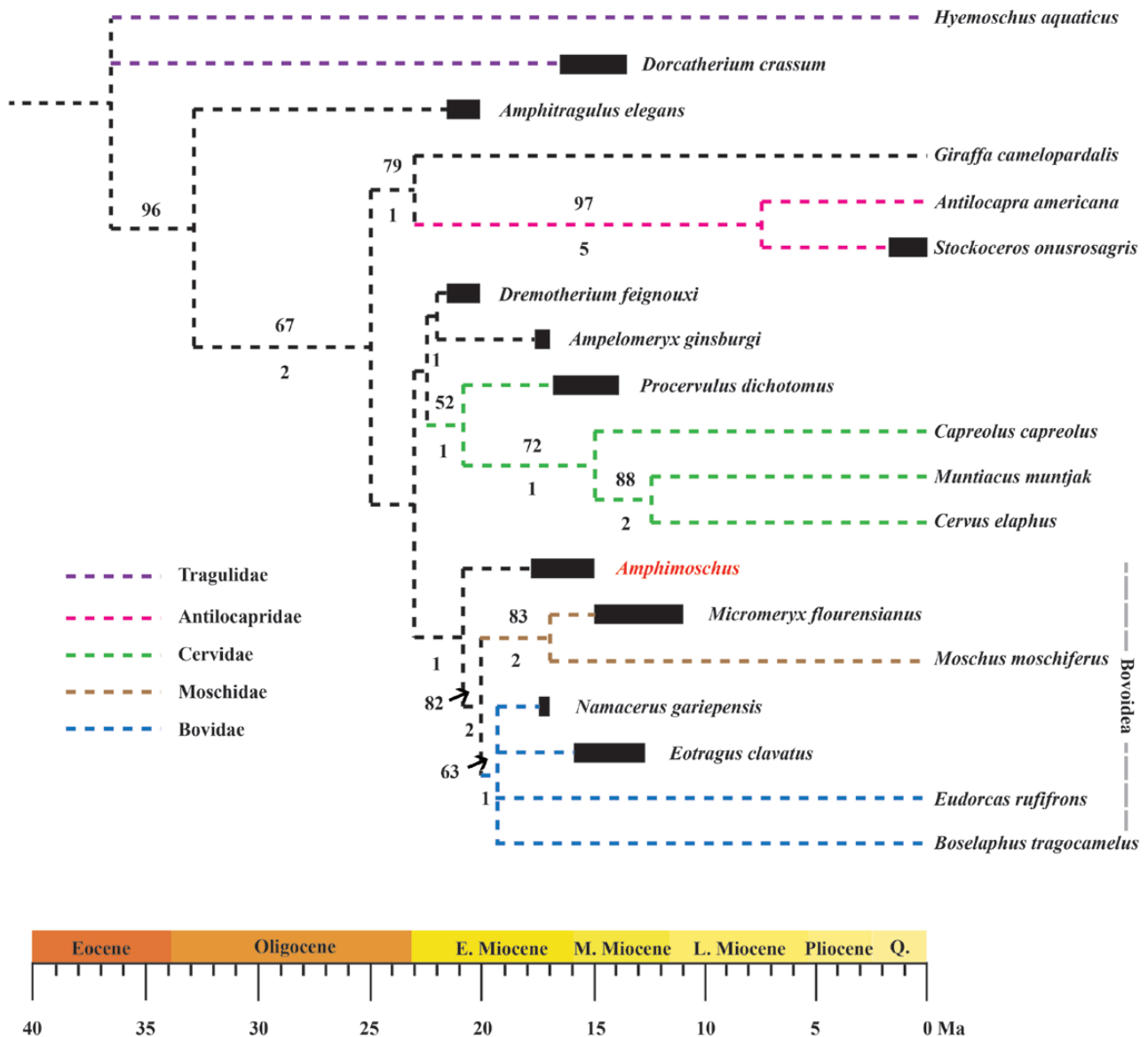
**Figure 4.** Strict consensus tree of nine most parsimonious trees, with 232 steps in PAUP (consistency index = 0.43; retention index = 0.59), indicating the systematic position of *Amphimoschus* as a basal member of the Bovoidea. Bremer supports (below) and bootstrap values ≥ 50% (above) are labelled at the corresponding nodes. Black bars indicate species chronological ranges.

and distinct frontal thickening on both sides. The antorbital protuberance, also seen in early dinoceratids and protoceratids (Osbon, 1913; Wheeler, 1961; Geist, 1966), could have functioned in lateral fighting behaviour with side head blows. The frontal thickening might have led to an increase in frontal support during heavy blows. The cranial integration is most likely to function in a similar manner to bovid horns in territorial behaviour (Lundrigan, 1996).

In order to shed more light on the early evolution of the Bovoidea, male territories of early bovoids were reconstructed using maximum likelihood based on the behavioural data of extant species and phylogenetic topology (Supporting Information, File S2, Table S1; Chen *et al.*, 2019). The most recent common ancestor of extant bovid and moschid species is equivalent to the latest stem bovoid. For this latest stem bovoid, the males established territories with 97.1% proportional likelihood. Furthermore, the assumption of males establishing territories was also statistically significant in the latest stem bovid (Fig. 5A). Hence, the latest stem bovoid and other bovoids during the late early Miocene (Chen *et al.*, 2019) were likely to establish territories.
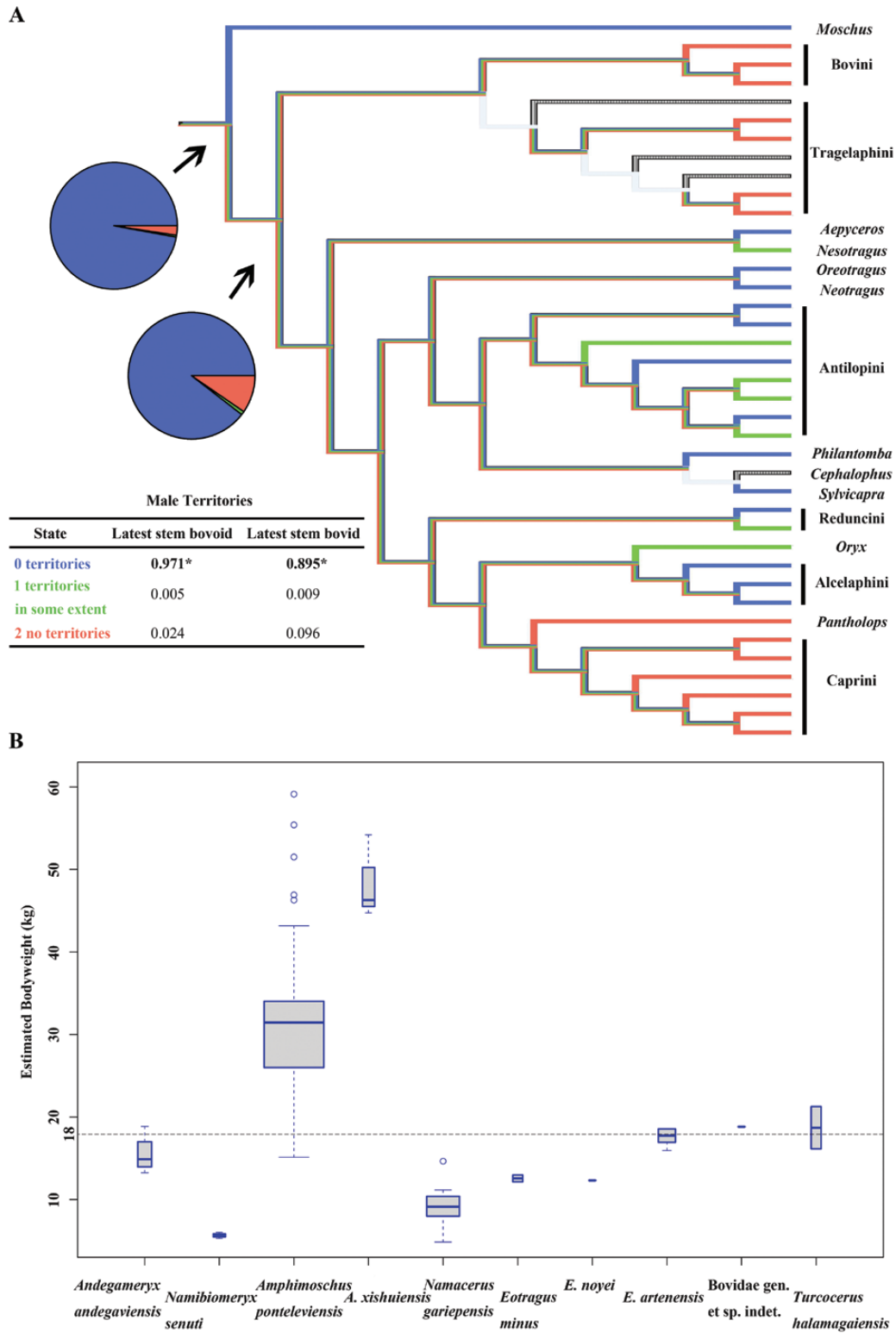
**Figure 5.** Behaviour and bodyweight of early bovoids. A, ancestral reconstruction of male territories of the latest stem bovoid and bovid (topology modified from Chen *et al.*, 2019). B, boxplot of bodyweight estimation of early bovoids (method and data seen in Supporting Information, File S2, Table S2). The box centre represents the median; box bounds represent the quartiles; whiskers represent maximum and minimum values (±1.5 × the interquartile range); open circles represent outliers; and the box width is proportional to the square root of the number of observations.

The origin and evolution of ruminant cranial appendages were proposed to be a metabolic response to increased seasonality, especially for foregut fermenters (Morales *et al.*, 1993), or considered as an inter-sex combat weapon with the acquisition of larger body sizes, for which 18 kg was defined as a critical weight to obtain enough nutrients from more fibrous sources of vegetation (Janis, 1982, 1990). A metabolic adjustment hypothesis might explain the presence of the entire pachyostosis or separate frontal thickening or frontal appendages. However, the weapon function hypothesis appears more suitable when the integrative cranial ornamentations of *A. xishuiensis* and general horn positions in bovids are considered (DeMiguel *et al.*, 2014; Allais-Bonnet *et al.*, 2021). Furthermore, the high probability of males establishing territories in early bovoids also fits well in this scenario. In any case, the 18 kg threshold seems not to be true for early bovoids (e.g. lower bodyweight present in *Namacerus* and some *Eotragus* species; Fig. 5B). Pecoran diversification is supposed to occur before the development of its cranial appendage (DeMiguel *et al.*, 2014; Sánchez *et al.*, 2015; Mennecart *et al.*, 2019). Before cranial appendage development, body size might have played an essential role in niche partitioning, because basal cervids and bovids adopted facultative mixed feeding strategies (DeMiguel *et al.*, 2008, 2012; Cantalapiedra *et al.*, 2014). At 19.5–17.0 Mya, vegetation resources might have become less nutritious and less abundant with low temperature fluctuation and low atmospheric $CO_2$ concentration (DeMiguel *et al.*, 2014; Cui *et al.*, 2020). Faunal turnovers and migrations may lead to the invasion of newcomers from different areas and an increase in competition (Morales *et al.*, 1993). For medium-sized early bovoids (Fig. 5B), the head blow rather than foreleg boxing might be more applicable (Jarman, 1974; DeMiguel *et al.*, 2014). Cranial appendages in Bovoidea might have brought advantages in intra- and interspecific competition and might further have brought an increase in diversification to groups of similar body sizes.

## REFERENCES

**Allais-Bonnet A**, **Hintermann A**, **Deloche M-C**, **Cornette R**, **Bardou P**, **Naval-Sanzhez M**, **Pinton A**, **Haruda A**, **Grohs C**, **Zakany J**, **Bigi D**, **Medugorac I**, **Putelat O**, **Greyvenstein O**, **Hadfield T**, **Jemaa SB**, **Bunevski G**, **Menzi F**, **Hirter N**, **Paris JM**, **Hedges J**, **Palhiere I**, **Rupp R**, **Lenstra JA**, **Gidney L**, **Lesur J**, **Schafberg R**, **Stache M**, **Wandhammer M-D**, **Arbogast R-M**, **Guintard C**, **Blin A**, **Boukadiri A**, **Rivière J**, **Esquerré D**, **Donnadieu C**, **Danchin-Burge C**, **Reich CM**, **Riley DG**, **Marle-Koster E**, **Cockett N**, **Hayes BJ**, **Drögenmüller C**, **Kijas J**, **Pailhoux E**, **Tosser-Klopp G**, **Duboule D**, **Capitan A. 2021.** Analysis of polycerate mutants reveals the evolutionary co-option of *HOXD1* for horn patterning in Bovidae. *Molecular Biology and Evolution* **38:** 2260–2272.

**Bärmann EV. 2014.** The evolution of body size, horn shape and social behaviour in crown Antilopini - an ancestral character state analysis. *Zitteliana B* **32:** 185–196.

**Bärmann EV**, **Rössner GE. 2011.** Dental nomenclature in Rumiantia: towards a standard terminological framework. *Mammalian Biology* **76:** 762–768.

**Barone R. 1999.** *Anatomie comparée des mammifères domestiques. Tome 1. Ostéologie*, 4th edn. Paris: Vigot.

**Bibi F. 2013.** A multi-calibrated mitochondrial phylogeny of extant Bovidae (Artiodactyla, Ruminantia) and the importance of the fossil record to systematics. *BMC Evolutionary Biology* **13:** 166.

**Bibi F. 2014.** Assembling the ruminant tree: combing morphology, molecules, extant taxa, and fossils. *Zitteliana B* **32:** 197–211.

**Bohlin B. 1946.** The fossil mammals from the Tertiary deposit of Taben-buluk, Western Kansu, Part II: Simplicidentata, Carnivora, Artiodactyla, Perissodactyla, and Primates. *Sino-Swedish Expedition Publication (Palaeontologia Sinica, New Series C, No. 8B)* **28:** 1–259.

**Bourgeois LA. 1873.** Note sur l'*Amphimoschus ponteleviensis*. *Journal de Zoologie* **2:** 235–236.

**Bubenik AB. 1990.** Epigenetical, morphological, physiological, and behavioral aspects of evolution of horns, pronghorns, and antlers. In: Bubenik GA, Bubenik AB, eds. *Horns, pronghorns, and antlers: evolution, morphology, physiology, and social significance*. New York: Springer-Verlag, 3–113.

**Cantalapiedra JL**, **FitzJohn RG**, **Kuhn TS**, **Fernández MH**, **DeMiguel D**, **Azanza B**, **Morales J**, **Mooers AØ. 2014.**

Dietary innovations spurred the diversification of ruminants during the Caenozoic. *Proceedings of the Royal Society B: Biological Sciences* **281:** 20132746.

**Castelló JR. 2016.** *Bovids of the world: antelopes, gazelles, cattle, goats, sheep, and relatives*. Princeton: Princeton University Press.

**Chen G-F**, **Wu W-Y. 1976.** Miocene mammalian fossils from Jiulongkou, Cixian, Hebei Province. *Vertebrata PalAsiatica* **14:** 6–19.

**Chen L**, **Qiu Q**, **Jiang Y**, **Wang K**, **Lin Z-S**, **Li Z-P**, **Bibi F**, **Yang Y-Z**, **Wang J-H**, **Nie W-H**, **Su W-T**, **Liu G-C**, **Li Q-Y**, **Fu W-W**, **Pan X-Y**, **Liu C**, **Yang J**, **Zhang C-Z**, **Yin Y**, **Wang Y**, **Zhao Y**, **Zhang C**, **Wang Z-K**, **Qin Y-L**, **Liu W**, **Wang B**, **Ren Y-D**, **Zhang R**, **Zeng Y**, **Fonseca RR**, **Wei B**, **Li R**, **Wan W-T**, **Zhao R-P**, **Zhu W-B**, **Wang Y-T**, **Duan S-C**, **Gao Y**, **Zhang YE**, **Chen C-Y**, **Hvilsom C**, **Epps CW**, **Chemnick LG**, **Dong Y**, **Mirarab S**, **Siegismund HR**, **Ryder OA**, **Gilbert MTG**, **Lewin HA**, **Zhang G-J**, **Heller R**, **Wang W. 2019.** Large-scale ruminant genome sequencing provides insights into their evolution and distinct traits. *Science* **364:** eaav6202.

**Cui Y**, **Schubert BA**, **Jahren AH. 2020.** A 23 m.y. record of low atmospheric $CO_2$. *Geology* **48:** 888–892.

**Davis EB**, **Brakora KA**, **Lee AH. 2011.** Evolution of ruminant headgear: a review. *Proceedings of the Royal Society B: Biological Sciences* **278:** 2857–2865.

**DeMiguel D**, **Azanza B**, **Morales J. 2014.** Key innovations in ruminant evolution: a paleontological perspective. *Integrative Zoology* **9:** 412–433.

**DeMiguel D**, **Fortelius M**, **Azanza B**, **Morales J. 2008.** Ancestral feeding state of ruminants reconsidered: earliest grazing adaptation claims a mixed condition for Cervidae. *BMC Evolutionary Biology* **8:** 13.

**DeMiguel D**, **Quiralte V**, **Azanza B**, **Montoya P**, **Morales J. 2012.** Dietary behaviour and competition for vegetal resources in two Early Miocene pecoran ruminants from Central Spain. *Geodiversitas* **34:** 425–443.

**Gagnaison C. 2017.** Le site paléontologique du Grand Morier (Pont-Boutard, Indre-et-Loire, France): contexte géologique et détail biostratigraphique des formations cénozoïques à partir des assemblages de vertébrés fossiles. *Geodiversitas* **39:** 251–271.

**Geist V. 1966.** The evolution of horn-like organs. *Behaviour* **27:** 175–214.

**Gentry AW. 1994.** The Miocene differentiation of old world Pecora (Mammalia). *Historical Biology* **7:** 115–158.

**Gentry AW**, **Heizmann EPJ. 1996.** Miocene ruminants of the Central and Eastern Tethys and Paratethys. In: Bernor RL, Fahlbusch V, Mittmann HW, eds. *The evolution of western Eurasian Neogene mammal fauna*. New York: Columbia University Press, 378–391.

**Gentry AW**, **Rössner GE**, **Heizmann EPJ. 1999.** Suborder Ruminantia. In: Rössner GE, Heissig K, eds. *The Miocene land mammals of Europe*. Munich: Dr. Friedrich Pfeil, 225–258.

**Ginsburg L. 2001.** Les faunes de mammifères terrestres du Miocène moyen des Faluns du basin de Savigné-sur-Lathan (France). *Geodiversitas* **23:** 381–394.

**Ginsburg L**, **Bonneau M. 1995.** La succession des faunes de mammifères miocènes de Pontigné (Maine-et-Loire, France).

*Bulletin du Muséum National d'Historie Naturelle* **16:** 313–328.

**Heizmann EPJ**, **Ginsburg L**, **Bulot C. 1980.** *Prosansanosmilus peregrinus*, ein neuer machairodontider Felide aus dem Miocän Deutschlands und Frankreichs. *Stuttgarter Beiträge zur Naturkunde Serie B* **58:** 1–28.

**Janis CM. 1982.** Evolution of horns in ungulates: ecology and paleoecology. *Biological Reviews of the Cambridge Philosophical Society* **57:** 261–317.

**Janis CM. 1990.** Correlation of reproductive and digestive strategies in the evolution of cranial appendages. In: Bubenik GA, Bubenik AB, eds. *Horns, pronghorns, and antlers: evolution, morphology, physiology, and social significance*. New York: Springer-Verlag, 114–133.

**Janis CM**, **Manning E. 1998.** Antilocapridae. In: Janis CM, Scott KM, Jacobs LL, eds. *Evolution of Tertiary mammals of North America, Vol. 1: terrestrial carnivores, ungulates, and ungulatelike mammals*. Cambridge: Cambridge University Press, 491–507.

**Janis CM**, **Scott KM. 1987.** The interrelationships of higher ruminant families with special emphasis on the members of the Cervoidea. *American Museum Novitates* **2893:** 1–85.

**Jarman PJ. 1974.** The social organisation of antelope in relation to their ecology. *Behaviour* **48:** 215–267.

**Li C-K**, **Lin Y-P**, **Gu Y-M**, **Hou L-H**, **Wu W-Y**, **Qiu Z-D. 1983.** The Aragonian vertebrate fauna of Xiaocaowan, Jiangsu-1. A brief introduction to the fossil localities and preliminary report on the new material. *Vertebrata PalAsiatica* **21:** 313–327.

**Li C-K**, **Qiu Z-D. 1980.** Early Miocene mammalian fossils of Xining basin, Qinghai. *Vertebrata PalAsiatica* **18:** 198–215.

**Li Y-K**, **Li Q**, **Ni X-J**, **Wang S-Q**, **Aiglstorfer M**, **Deng T. 2021a.** The oldest known bovid from China and reappraisal of the Chinese '*Eotragus*'. *Papers in Palaeontology* **7:** 913–929.

**Li Y-K**, **Mennecart B**, **Aiglstorfer M**, **Ni X-J**, **Li Q**, **Deng T. 2021b.** 3D models related to the publication: The early evolution of cranial appendages in Bovoidea revealed by new species of *Amphimoschus* (Mammalia: Ruminantia) from China. *MorphoMuseuM*. doi:10.18563/journal.m3.151

**Lundrigan B. 1996.** Morphology of horns and fighting behavior in the Family Bovidae. *Journal of Mammalogy* **77:** 462–475.

**Maddison WP**, **Maddison DR. 2018.** *Mesquite: a modular system for evolutionary analysis, Version 3.40*. Available at: http://mesquiteproject.org

**Matthews SC. 1973.** Notes on open nomenclature and on synonymy lists. *Palaeontology* **16:** 713–719.

**Mayet L. 1908.** Étude des mammifères Miocènes des sables de L'Orléanais et des faluns de la Touraine. *Annales de L'Université de Lyon* **24:** 1–336.

**Mazza PPA. 2013.** The systematic position of Hoplitomerycidae (Ruminantia) revisited. *Geobios* **46:** 33–42.

**Mennecart B**, **DeMiguel D**, **Bibi F**, **Rössner GE**, **Metais G**, **Neenan JM**, **Wang S-Q**, **Schultz G**, **Müller B**, **Costeur L. 2017.** Bony labyrinth morphology clarifies the origin and evolution of deer. *Scientific Reports* **7:** 13176.

**Mennecart B**, **Métais G**, **Costeur L**, **Ginsburg L**, **Rössner GE. 2021.** Reassessment of the Miocene genus *Amphimoschus* Bourgeois, 1873 (Mammalia, Artiodactyla, Ruminantia, Pecora). *PLoS One* **16:** e0244661.

**Mennecart B**, **Zoboli D**, **Costeur L**, **Pillola GL. 2019.** On the systematic position of the oldest insular ruminant *Sardomeryx oschiriensis* (Mammalia, Ruminantia) and the early evolution of the Giraffomorpha. *Journal of Systematic Palaeontology* **17:** 691–704.

**Morales J**, **Pickford M**, **Soria D. 1993.** Pachyostosis in a Lower Miocene giraffoid from Spain, *Lorancameryx pachyostoticus* nov. gen. nov. sp. and its bearing on the evolution of bony appendages in artiodactyls. *Geobios* **26:** 207–230.

**Mörs T**, **Von der Hocht F**, **Wutzler B. 2000.** Die erste Wirbeltierfauna aus der miozänen Braunkohle der Niederrheinischen Bucht (Ville-Schichten, Tagebau Hambach). *Paläontologische Zeitschrift* **74:** 145–170.

**Osbon HF. 1913.** The skull of *Bathyopsis*, wind river uintathere. *Bulletin of the American Museum of Natural History* **32:** 417–426.

**Qiu Z-X**, **Qiu Z-D. 2013.** Early Miocene Xiejiahe and Sihong fossil localities and their faunas, eastern China. In: Wang X-M, Flynn LJ, Fortelius M, eds. *Fossil mammals of Asia: Neogene biostratigraphy and chronology*. New York: Columbia University Press, 142–154.

**Qiu Z-X**, **Qiu Z-D**, **Deng T**, **Li C-K**, **Zhang Z-Q**, **Wang B-Y**, **Wang X-M. 2013.** Neogene land mammal stages/ages of China: toward the goal to establish an Asian land mammal stage/age scheme. In: Wang X-M, Flynn LJ, Fortelius M, eds. *Fossil mammals of Asia: Neogene biostratigraphy and chronology*. New York: Columbia University Press, 29–90.

**Qiu Z-X**, **Yan D-F**, **Jia H**, **Sun B. 1985.** Preliminary observations on the newly found skeletons of *Palaeomeryx* from Shanwang, Shandong. *Vertebrata PalAsiatica* **23:** 173–200.

**Roman F**, **Viret J. 1934.** La faune de mammifères du burdigalien de La Romieu. *Mémoires de la Société Géologique de France NS* **21:** 5–67.

**Rössner GE**, **Bärmann EV**, **Heckeberg NS**, **Asher RJ**, **Erpenbeck D**, **Wörheide G. 2013.** On the phylogenetic position of the hornless pecoran *Amphimoschus* – an example of arising challenges with the incorporation of fossils in extant combined frameworks. *Zitteliana* **31:** 30–31.

**Sach VVJ**, **Heizmann EPJ. 2001.** Stratigraphie und Säugetierfaunen der Brackwassermolasse in der Umgebung von Ulm (Südwestdeutschland). *Stuttgarter Beiträge zur Naturkunde Serie B* **310:** 1–95.

**Sánchez IM**, **Cantalapiedra JL**, **Ríos M**, **Quiratle V**, **Morales J. 2015.** Systematics and evolution of the Miocene three-horned Palaeomerycid ruminants (Mammalia, Cetartiodactyla). *PLoS One* **10:** e0143034.

**Sánchez IM**, **Domingo MS**, **Morales J. 2010.** The genus *Hispanomeryx* (Mammalia, Ruminantia, Moschidae) and its bearing on musk deer phylogeny and systematics. *Palaeontology* **53:** 1023–1047.

**Scherler L**, **Mennecart B**, **Hiard F**, **Becker D. 2013.** Evolutionary history of hoofed mammals during the Oligocene–Miocene transition in Western Europe. *Swiss Journal of Geosciences* **106:** 349–369.

**Swofford DL. 2002.** *PAUP*: phylogenetic analysis using parsimony (*and other methods), Version 4*. Sunderland: Sinauer Associates.

**Vislobokova IA. 1997.** Eocene–Early Miocene ruminants in Asia. In: Aguilar JP, Legendre S, Michaux J, eds. *Actes du Congrès BiochroM'97, Mémoires et Travaux*. Montpellier: l'École Pratique des Hautes Etudes, Institut de Montpellier, 215–223.

**Wang B-Y. 2002.** Dipodidae (Rodentia, Mammalia) from the Mid-Tertiary deposits in Danghe area, Gansu, China. *Vertebrata PalAsiatica* **41:** 89–103.

**Wang B-Y**, **Qiu Z-X. 2002.** A new species of *Platybelodon* (Gomphotheriidae, Proboscidea, Mammalia) from Early Miocene of the Danghe area, Gansu, China. *Vertebrata PalAsiatica* **40:** 291–299.

**Wang X-M**, **Li Q**, **Qiu Z-D**, **Xie G-P**, **Wang B-Y**, **Qiu Z-X**, **Tseng ZJ**, **Takeuchi GT**, **Deng T. 2013.** Neogene mammalian biostratigraphy and geochronology of the Tibetan Plateau. In: Wang X-M, Flynn LJ, Fortelius M, eds. *Fossil mammals of Asia: Neogene biostratigraphy and chronology*. New York: Columbia University Press, 274–292.

**Wang X-M**, **Qiu Z-D**, **Li Q**, **Tomida Y**, **Kimura Y**, **Tseng ZJ**, **Wang H-J. 2009.** A new Early to Late Miocene fossiliferous region in Central Nei Mongol: lithostratigraphy and biostratigraphy in Aoerban Strata. *Vertebrata PalAsiatica* **47:** 111–134.

**Wang X-M**, **Qiu Z-D**, **Wang B-Y. 2004.** A new leptarctine (Carnivora: Mustelidae) from the early Miocene of the northern Tibetan Plateau: implications for the phylogeny and zoogeography of basal mustelids. *Zoological Journal of the Linnean Society* **142:** 405–421.

**Wang X-M**, **Wang B-Y**, **Qiu Z-X. 2008.** Early explorations of Tabenbuluk Region (western Gansu Province) by Birger Bohlin—reconciling classic vertebrate fossil localities with modern stratigraphy. *Vertebrata PalAsiatica* **46:** 1–19.

**Wang X-M**, **Wang B-Y**, **Qiu Z-X**, **Xie G-P**, **Xie J-Y**, **Downs W**, **Qiu Z-D**, **Deng T. 2003.** Danghe area (western Gansu, China) biostratigraphy and implications for depositional history and tectonics of northern Tibetan Plateau. *Earth and Planetary Science Letters* **208:** 253–269.

**Wang Y**, **Zhang C-Z**, **Wang N-N**, **Li Z-P**, **Heller R**, **Liu R**, **Zhao Y**, **Han J-G**, **Pan X-Y**, **Zheng Z-Q**, **Dai X-Q**, **Chen C-S**, **Dou M-L**, **Peng S-J**, **Chen X-Q**, **Liu J**, **Li M**, **Wang K**, **Liu C**, **Li Z-S**, **Chen L**, **Hao F**, **Zhu W-B**, **Song C-C**, **Zhao C**, **Zheng C-L**, **Wang J-M**, **Hu S-W**, **Li C-Y**, **Yang H**, **Jiang L**, **Li G-Y**, **Liu M-J**, **Sonstegard TS**, **Zhang G-J**, **Jiang Y**, **Wang W**, **Qiu Q. 2019a.** Genetic basis of ruminant headgear and rapid antler regeneration. *Science* **364:** eaav6335.

**Wang Y-F**, **Wei C-F**, **Que J-M**, **Zhang W-D**, **Sun C-L**, **Shu Y-F**, **Hou Y-M**, **Zhang J-C**, **Shi R-J**, **Wei L. 2019b.** Development and applications of paleontological computed tomography. *Vertebrata PalAsiatica* **57:** 84–92.

**Wheeler WH. 1961.** Revision of the uintatheres. *Peabody Museum of Natural History Yale University Bulletin* **14:** 1–93.

## SUPPORTING INFORMATION

Additional Supporting Information may be found in the online version of this article at the publisher's web-site:

**File S1.** Data matrix of 19 species and 68 characters for the phylogenetic analysis.
**File S2: Figure S1.** Strict consensus tree of nine most parsimonious trees with 232 steps in PAUP (consistency index = 0.43; retention index = 0.59). Open circles indicate homoplasic synapomorphy, and black circles indicate strict synapopmorphy.
**Table S1.** Male territories of 39 extant bovoid species.
**Table S2.** Bodyweight estimation of early bovoids.